

Creation of stable water-free antibody based protein liquids

Joseph M. Slocik¹, Patrick B. Dennis¹, Zhifeng Kuang¹, Anthony Pelton¹ & Rajesh R. Naik²  

Antibodies represent highly specific and high binding affinity biomolecular recognition elements for diagnostic assays, biosensors, and therapeutics, but are sensitive to denaturation and degradation. Consequently, the combination of existing in a hydrated state with a large and complex biomolecular structure results in loss of antibody-antigen binding, limited shelf-life, and decreased sensor response over time and under non-optimal conditions. The development and use of water-free protein liquids has led to stabilization of labile biomolecules, solvents for biotransformation reactions, and formation of new bio-composites with incompatible materials. Here, we exploit the polycationic nature of modified antibodies and their ability to form ion pairs for the conversion of primary Immunoglobulin G antibodies into stable protein liquids that retained more than 60% binding activity after repeated heating up to 125 °C, and demonstrate compatibility with thermoplastics.

¹ Materials and Manufacturing Directorate, Air Force Research Laboratory, Wright-Patterson AFB, Dayton, OH 45433, USA. ² 711 Human Performance Wing, Air Force Research Laboratory, Wright-Patterson AFB, Dayton, OH 45433, USA. ✉email: Rajeshnaik.phd@gmail.com

The successful integration of biological materials in biosensors, diagnostics, biomedical devices, and other abiotic materials (e.g., plastics) is severely limited by the poor stability of biomolecules, low tolerance to elevated temperatures, and increased sensitivity and incompatibility issues due to different processing conditions (i.e., pH, salts, solvents) resulting in loss of biofunctionality. In all, these issues restrict the utilization of biological materials in operational and real-world settings without the use of strictly controlled environmental conditions (e.g., refrigeration) and/or the need for multiple processing steps. Consequently, to date, there has been limited progress toward device integration, achieving thermal stabilization, and in improving the processibility of biomolecules^{1,2}.

In particular, antibodies exemplify the need to overcome these inherent limitations for effective utilization and device integration. Generally, antibodies require aqueous environments and physiological conditions (neutral pH, ambient temperatures 25–37 °C) in order to perform their biological function^{3–6}. Of these requirements, water is essential for stabilizing biomolecular structures through hydrogen bonding, providing proton donors/acceptors, regulating binding interactions, and controlling molecular dynamics; but, at the same time, water is very detrimental to biomolecular structure and function by increasing the rate of hydrolysis and oxidation, destabilizing and disrupting protein structure, and increasing the susceptibility/sensitivity to elevated temperatures. To counteract the effects of water and limit decomposition, antibodies require constant refrigeration during storage/handling/transport to slow the rate of hydrolysis, preserve structure, functionality, and biological activity. Based on general guidelines for the storage of antibodies, aqueous antibodies are stable for up to 1 month when stored at 4 °C and up to 1 year in 25% glycerol at –20 °C⁷. The need for refrigeration poses a major barrier for resource-limited regions which lack widespread electricity, proper infrastructure, and adequate health services; as well as for military medvac operations where equipment weight and accessibility are considerable tactical concerns. Consequently, the exclusion of water from antibody preparations is highly appealing and offers a means toward reducing protein degradation, increasing stability, enabling refrigeration-free storage and handling, and significantly increasing antibody shelf-life. To date, there have been extensive efforts directed at minimizing refrigeration requirements, eliminating the need for a cold-chain, achieving room temperature storage, and incrementally increasing shelf-lives. Examples of stabilization include encapsulation of antibodies in silk or MOFs^{8–11}, use of additives or stabilizers¹², coacervation of antibodies^{13,14}, use of alternate types of antibodies (single-domain antibodies from camelids)¹⁵, and development of non-natural molecularly imprinted artificial antibodies¹⁶. All of these enhance room temperature storage and/or prolong shelf-lives, but at the disadvantage of containing a significant amount of trapped water and resulting in lower thermal tolerance.

Alternatively, solvent-free protein liquids feature the simplicity of traditional small molecule ionic liquids (facile synthesis, ability to tune properties through choice of cation and anion pair, and stability), but display the complexity and functionality of highly active proteins. Because protein liquids are devoid of water^{17,18}, they represent stable liquids which are resistant to extreme temperatures (>100 °C), able to maintain biological activity, and exhibit much longer shelf-lives without the need for refrigeration^{19–21}. Solvent-free protein liquids have been created using ferritin, M13 bacteriophage, avidin, glucose oxidase, BSA, lysozyme, lipase, myoglobin, DNA, a plant virus, and an assortment of other mesophilic enzymes^{20,22–33}.

In this study, we combined the physical properties of protein liquids and biological recognition of primary antibodies to create a stable and heat resistant antibody protein liquid that promises

refrigeration-free storage and high-temperature processing with abiotic materials³⁴. As a result, water-free antibody liquids exhibited >60% binding activity after repeated heating to 125 °C and facilitated the creation of antibody-based hot glue materials.

Results and discussion

Antibody modification. Polyclonal rabbit anti-ferritin immunoglobulin G (anti-ferritin IgG) antibodies or IgG antibodies obtained from rabbit serum (IgG) were cationized by the addition of N,N-dimethyl-1,3-propanediamine (DMPDA) in the presence of 1-ethyl-3-(3-dimethylaminopropyl)carbodiimide (EDC) coupling reagent in order to modify carboxyl containing amino acids (aspartic and glutamic acid) with positive charges. EDC-based coupling reactions are highly specific for the covalent coupling of amine to carboxyl groups and proceed by activation of carboxyl group to an ester and formation of an amide bond³⁵. For example, this process has been effectively used to produce supercharged variants of GFP³⁶. Similarly, we modified the acidic residues of primary IgG antibodies from rabbit serum or anti-ferritin IgG antibodies (rabbit) with positively charged DMPDA and then experimentally determined the addition of positive charges by zeta potential measurements and MALDI mass spectrometry. To provide a baseline, rabbit IgG exhibited a zeta potential of $+12.7 \pm 0.7$ mV at neutral pH that is consistent with a prevalence of basic amino acids (198/1320 total) in the primary sequence of rabbit IgG (Fig. 1a)³⁷. Bookkeeping of available acidic residues reveals a rabbit IgG molecule composed of 2 light chains and 2 heavy chains contains a total of 96 acidic amino acids/1320 amino acids that are modifiable³⁷. However, we expect some of these residues will be buried and inaccessible for modification. As a result, we used an empirical approach to determine how many acidic residues are inaccessible within an antibody structure. We selected the human antibody IgG1 b12 as a surrogate model, since its crystal structure is resolved at 2.7 Å (pdb access code 1hzh), contains 122 acidic residues (vs. 98 in rabbit), and shares a conserved structure to rabbit IgG with the exception of a small flexible hinge region^{38,39}. Based on this empirical approach, a residue is regarded as buried if a sphere with a radius of 15 Å is located at the mass center of a residue containing more than 560 heavy atoms (Supplementary Fig. 1). Using this criterion, we found that ASP115, GLU367, and ASP386 (residue number follows FASTA sequences published at pdb databank) within each heavy chain are buried. In total, this accounts for 6 acidic residues buried below the IgG surface that are inaccessible for modification out of a possible 122 available residues. By analogy, we estimate that up to 6 residues within rabbit IgG are inaccessible for modification. Consequently, the cationization of rabbit IgG (C-IgG) was reflected by a much higher zeta potential ($+36.3 \pm 4.7$ mV) and a slight increase in the average diameter (number %) from 9.0 ± 2.7 nm to 12.1 ± 2.8 nm by dynamic light scattering (DLS) (Fig. 1b, Supplementary Fig. 2). MALDI mass spectrometry confirmed the addition of 32 positive charges per C-IgG antibody distributed over the light and heavy chains (Supplementary Fig. 3). Overall, the addition of positive charges represents modifications to only 2.5% of the total antibody, but importantly, results in an increase in surface charge density covalently added on the exterior antibody surface.

Synthesis and characterization of water-free antibody liquid.

To form the corresponding antibody liquid, anionic polymer surfactants of poly(ethylene glycol) 4-nonylphenyl 3-sulfopropyl ether [S] are added to the C-IgG component by means of electrostatic complexation in order to balance charges and produce a neutral protein salt. To determine the number of [S] anions that interact with antibody charges, we measured the zeta potential of

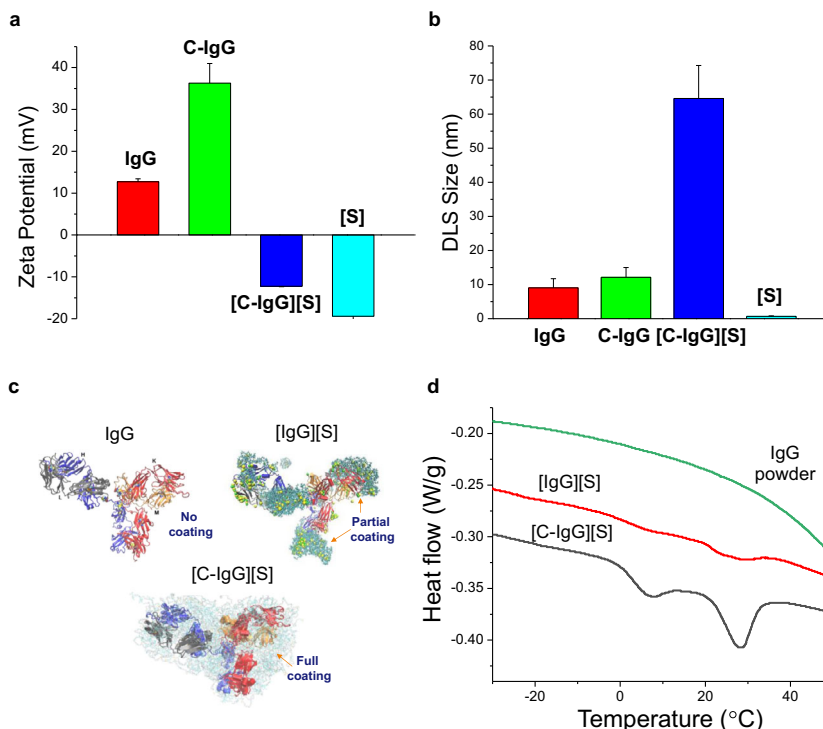


Fig. 1 Characterization of antibody liquid. **a** Zeta potential measurements of rabbit IgG antibodies after cationization (C-IgG) and complexation with anions [C-IgG][S]. Error bars represent the standard deviation from three separate measurements. **b** Dynamic Light Scattering (DLS) plot of rabbit IgG antibodies after cationization (C-IgG) and complexation with anions [C-IgG][S]. Error bars represent the standard deviation from three separate measurements. **c** Molecular structures of IgG antibodies, IgG with anions of [S] added (labeled [IgG][S]), and [C-IgG][S] antibody liquid obtained after 200 ns of molecular dynamics simulations. **d** Differential scanning calorimetry (DSC) plot of [C-IgG][S], IgG powder only, and [IgG][S] at 1:4 wt ratio.

IgG from rabbit serum or C-IgG upon titration with [S] anions. From the titration plots, we determined ~ 176 anions of [S] per IgG and ~ 195 anions per C-IgG antibody are required to balance charges and reach charge neutrality (Supplementary Fig. 4). Collectively, this represents multiple types of antibody-anion interactions that span different ionic binding strengths¹³. The magnitude of these interactions is influenced by different amino acids (arginine and lysine), type of charge (tertiary and primary amines), and a large assortment of pK_a 's. This is reflected by different slopes in the zeta potential titration plots of C-IgG or IgG and lower numbers of complexed anions. Consequently, we added 370 anions of [S] to C-IgG (3:1 wt ratio) to form the [C-IgG][S] conjugate. This ratio was selected based on previous protein liquids and because it represents an excess of anions. An excess was required to reach saturated conjugation of [S] and a full wrapping around C-IgG due to steric influences. After dialysis to remove non-interacting anions, we determined that C-IgG was associated with 305 anions of [S] based on zeta potential of the final material and extrapolation from titration plot (Fig. 1a). By comparison, this is in good agreement with 230 theoretical positive charges on rabbit C-IgG. In addition, DLS showed an increase in the average diameter of C-IgG antibodies (12.1 ± 2.8 nm) in the presence of anionic polymers of [S] to create [C-IgG][S] (64.6 ± 9.6 nm) (Fig. 1b, Supplementary Fig. 2). This larger size is likely attributed to the random association of anionic polymer shells from multiple [C-IgG][S] conjugates and/or a propensity of rabbit IgG to form multimers at high antibody and salt concentrations³⁷. Consequently, the [C-IgG][S] liquid satisfies both of these conditions for formation of multimers. The [C-IgG][S] complex was lyophilized to remove all water content and melted under mild heating to form a viscous translucent liquid. DSC of the [C-IgG][S] conjugate revealed a weak glass transition temperature at ~ 7 °C and an intense endothermic peak

at ~ 28 °C indicative of melting and similar to other solvent-free protein liquids²⁶. DSC of the lyophilized IgG powder and a partially wrapped IgG (native rabbit IgG antibody with anion at 1:4 wt ratio) showed a broad exotherm and diminished endothermic peaks, respectively (Fig. 1c, d). Notably, the partially wrapped rabbit IgG failed to melt into a liquid due to the lower number of antibody-polymer interactions and presence of multiple exposed regions lacking anions.

The tolerance of antibodies to cationization and complexation with anionic polymers of [S] was determined by measuring the secondary structure and binding affinity of anti-ferritin IgG antibodies. Structurally, the circular dichroism (CD) spectrum of IgG showed a peak with negative ellipticity at 218 nm that is characteristic of a β -sheet structure and consistent with the CD spectra of other IgG's (Supplementary Fig. 5)⁴⁰. After cationization and complexation, the CD peak slightly shifted to ~ 219 nm and lost ellipticity signifying a minor change in secondary structure. In all, these structural changes are similar to other solvent-free protein liquids³⁰. By comparison to anti-ferritin IgG antibodies ($K_D = 1.2 \times 10^{-10}$ M), we obtained similar dissociation constants for the [anti-ferritin C-IgG][S] equal to 4.1×10^{-10} M, respectively, using QCM (Supplementary Fig. 6). This confirms that cationization of surface-exposed acidic residues did not affect the binding affinity of [anti-ferritin C-IgG][S] to apoferritin. Also, this suggests that stabilizing anions of [S] dissociate from the [anti-ferritin C-IgG][S] upon reconstitution in aqueous solution and/or are readily displaced by stronger antigen-binding interactions. In nature, antibodies are also commonly modified by means of glycosylation *in vivo* to increase longevity and stability⁴¹. To determine the effects of cationization and complexation with anions of [S] on binding specificity, we also used an Ouchterlony double diffusion technique to detect formation of an immune complex with anti-ferritin C-IgG or

[anti-ferritin C-IgG][S] via immunoprecipitation. Ouchterlony double diffusion is commonly used to detect the formation of an immune complex between antigens and antibodies via immunoprecipitation and to provide insight about the identity of unknown antigens^{42,43}. A typical format for an Ouchterlony assay involves using a central pre-cut well for antibody diffusion surrounded by 6 pre-cut wells for co-diffusion of multiple antigens. Notably, this diffusion format enables the determination of antigen identity with respect to neighboring antigens bearing unknown epitope identities. Similarly, we used this concept of antigen identity to evaluate the effects of antibody modifications on the specificity of binding interactions (e.g., cationization and complexation with anions) by utilizing the central well for antigen diffusion and the surrounding wells to represent different antibody modifications and conditions. Conceptually, the intersection of adjacent immunoprecipitation lines between antigen wells is reliably used to reveal the extent of identity of epitope binding sites on multiple antigens (i.e., fully identical, partially identical, or non-identical) (Supplementary Fig. 7). For example, two intersecting immunoprecipitation lines that cross each other are indicative of antigens that are non-identical; while immunoprecipitation lines that meet and do not cross are classified as being fully identical antigens. Briefly, we obtained a series of thin white lines in the gel signifying antigen recognition and formation of immune complexes. In total, we detected immunoprecipitation complexes with combinations of apoferritin and anti-ferritin C-IgG only, anti-ferritin IgG only, and [anti-ferritin C-IgG][S] liquid at room temperature (Supplementary Fig. 7). For these complexes, the presence of intersecting and non-crossing immunoprecipitation lines confirms the fully identical binding nature of anti-ferritin C-IgG and [anti-ferritin C-IgG][S] with respect to anti-ferritin IgG and binding interactions with apoferritin antigen. In contrast, we did not observe visual precipitation bands for the anions of [S] only, a nonspecific mouse monoclonal antibody against Interleukin 6, and anti-ferritin IgG antibody heated at 100 °C. However, [anti-ferritin C-IgG][S] liquid heated at 100 °C performed similarly to native antibodies confirming the tolerance of antibody ionic liquids to extreme heating.

Thermal stability of water-free antibody liquids. A significant feature of nanoscale protein liquids is their resistance to extreme temperatures due to the absence of water and presence of a dense polymer anion shell protecting the C-IgG. The removal of water eliminates hydrolysis, creates favorable enthalpic contributions, and leads to increased intramolecular binding interactions and forces within the protein interior (i.e., Hydrogen bonding and Van der Waals interactions). Consequently, anti-ferritin IgG, anti-ferritin IgG with [S] anions added, and [anti-ferritin C-IgG][S] were heated to 125 °C and measured for binding to apoferritin by QCM and a dot blot assay. QCM is commonly used to measure antibody-antigen binding, test and validate the performance of immunosensors, and assess the efficacy of antibody stabilizers^{12,44,45}. Using QCM, we precisely quantitated the loss/preservation of binding activity as a function of increasing temperatures by measuring the mass of antigen immobilized on the surface of a gold-coated QCM sensor and the mass of bound antibody. From QCM measurements, we determined binding stoichiometries from the mass ratio of antigen to bound antibody (Supplementary Fig. 8). Consequently, the native aqueous antibody (stored at 4 °C) revealed a binding stoichiometry of ~6 antibodies (anti-ferritin IgG) per apoferritin protein consistent with multi-valent binding to 24 identical protein subunits. This was used as a baseline and reference value to calculate the loss/preservation of binding activity of antibodies after heating at

subsequent temperatures. The thermal stability of aqueous anti-ferritin IgG or lyophilized anti-ferritin IgG was determined by individually exposing antibodies to temperatures of 25, 50, 75, and 100 °C for 30 min and measuring their binding by QCM to an apoferritin protein-coated sensor (Fig. 2a). Based on these physical states, the aqueous form estimates the pot-life of antibodies, while the lyophilized antibody powder estimates shelf-life and is more comparable to the water-free antibody liquid. At 75 and 100 °C exposures, aqueous anti-ferritin IgG lost 70% and 90% of its binding activity, respectively, to yield a T_m of 65 °C; while the lyophilized form lost 60% of its binding after heating to only 50 °C (Fig. 2a). This loss in binding activity was confirmed by dynamic light scattering (DLS) and revealed that the average size of the aqueous antibody increased from 11 nm to ~250 nm after heating at 100 °C indicative of antibody unfolding and aggregation (Supplementary Fig. 9). By comparison, the water-free antibody liquid form of anti-ferritin C-IgG showed increased stability >100 °C as determined by a loss of only ~10% of its binding activity at 100 °C and ~35% when heated to 125 °C using the same sample for all heating (Fig. 2a). The use of the same sample was necessary because of difficulties in consistently measuring and dispensing accurate amounts of highly viscous antibody liquid. To determine thermal stability at multiple temps using the same sample, [anti-ferritin C-IgG][S] was heated in the water-free state, reconstituted to measure binding, frozen at -80 °C, lyophilized to remove water, exposed to a higher temperature in water-free state, and repeated for all temps. By comparison to controls, the binding affinities are artificially lower due to use of a single sample for all measurements, but notably, demonstrates the reusability of antibody liquids and ability to be cycled between storage in the dry state and reconstituted aqueous forms (Supplementary Fig. 10). In addition, the antibody liquid was subjected to large temperature swings (-80 to 100 °C) in order to simulate extreme conditions.

In parallel, we also used immunoblotting to qualitatively determine binding of antibody liquids of [anti-ferritin C-IgG][S] after heating. For immunoblotting, different concentrations of apoferritin (10 pM to 1 μ M) were immobilized on a nitrocellulose membrane, blocked with 1% milk, incubated with [anti-ferritin C-IgG][S] or anti-ferritin IgG antibody, washed extensively with buffer, incubated with a secondary goat anti-rabbit (GAR) antibody conjugated with alkaline phosphatase, washed, and developed using colorimetric substrate. Qualitatively, both the reconstituted [anti-ferritin C-IgG][S] and aqueous anti-ferritin IgG antibody at room temperature showed binding and detection of apoferritin at the lowest concentration of 10 pM (Fig. 2b, Supplementary Fig. 11). However, after heating to 100 °C, only [anti-ferritin C-IgG][S] showed binding to apoferritin (Fig. 2b, Supplementary Fig. 11). Notably, this also confirms that binding of secondary goat anti-rabbit antibodies to the F_c region of [anti-ferritin C-IgG][S] is similarly unaffected by cationization or complexation with anions of [S].

Molecular modeling of water-free antibody liquids. We have further investigated the thermal stability and functional mechanism of rabbit [C-IgG][S] at the molecular level using molecular modeling techniques and a surrogate antibody. We have again utilized the human antibody IgG1 b12 (pdb access code 1hzh) to investigate the effect of cationization, complexation with anions of [S], and formation of a water-free antibody liquid on the thermal stability and molecular structure of IgG. Solvating the crystal structure of IgG in TIP3 water (Supplementary Fig. 12), we determined the equilibrated IgG antibody structure after 200 ns of molecular dynamics simulation at 25 °C (Fig. 1c) by monitoring the time evolution of the radius of gyration

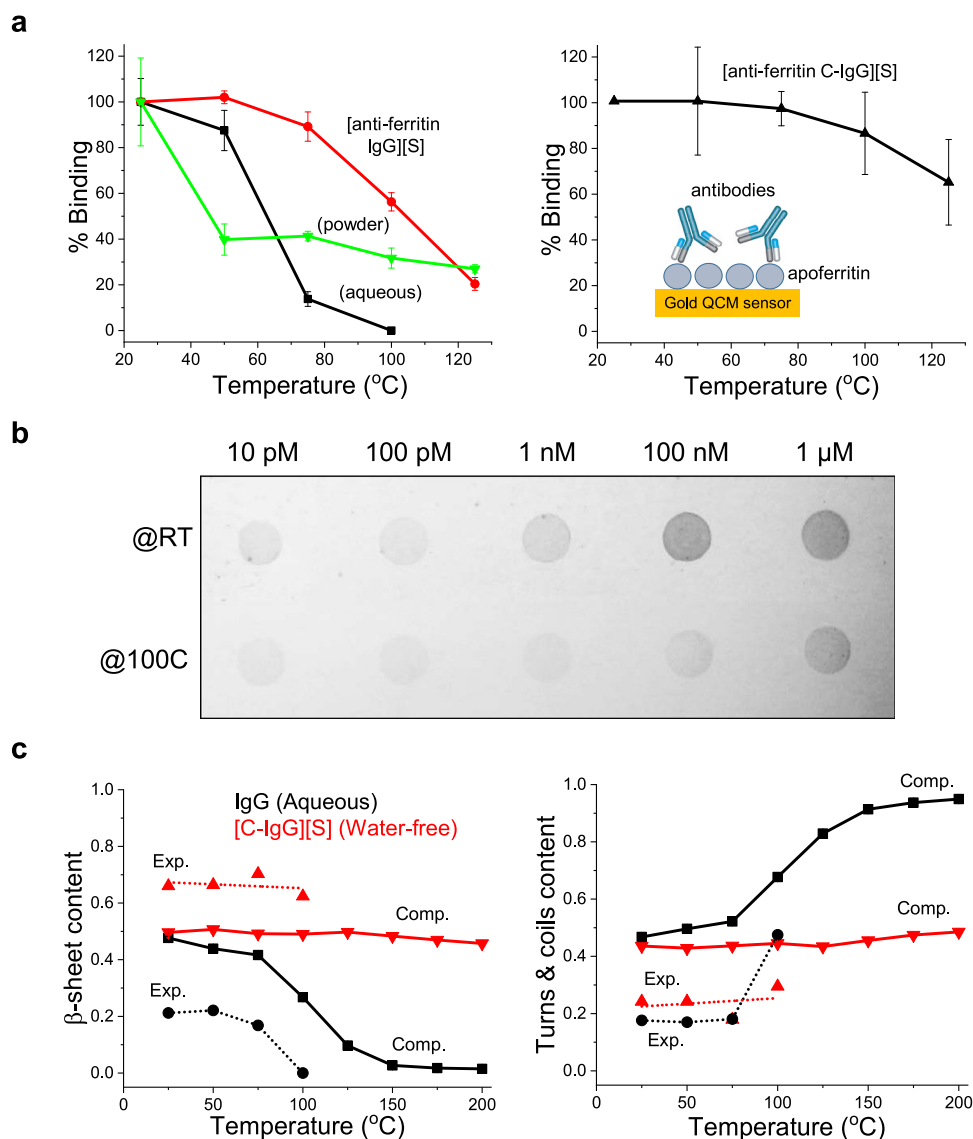


Fig. 2 Thermal stability of antibody liquids. **a** Quartz Crystal Microbalance (QCM) binding of anti-ferritin in aqueous and powder forms and [anti-ferritin IgG][S] at 1:4 wt ratio after heating (Left plot). Binding of [anti-ferritin C-IgG][S] after repeated heating of same sample (Right plot). Inset shows QCM binding exp. % Binding was determined from conversion of Δf into an aerial mass (ng/cm^2) of adsorbed apoferritin and bound antibody using the Sauerbrey equation and then into a mole ratio. Error bars represent the standard deviation of three separate binding experiments. **b** Immunoblot binding assay of [anti-ferritin C-IgG][S] at RT and at 100 °C with 10 pM to 1 μM apoferritin developed colorimetrically with GAR-AP secondary antibodies. **c** Secondary structure changes of IgG and [C-IgG][S] at equilibria and at different temperatures determined by molecular modeling simulations (labeled comp) and experimentally (labeled exp). Error bars from MD simulations are included in plot and determined from 50 snapshots using VMD. Secondary structure content was also experimentally determined by deconvolution of CD spectra for aqueous IgG and by peak fitting the Amide I band in FT-IR spectra (reflection mode) of water-free [C-IgG][S] to known secondary structure vibrational modes. For IgG, only the turn content is represented experimentally.

(Supplementary Fig. 12f). This equilibrated structure of IgG was used as the reference structure to compare the thermal stability under different conditions. First, the equilibrated structure of IgG without modification was further equilibrated at eight different temperatures (25:25:200 °C) using the generalized Born implicit solvent to save simulation time, denoted as IgG in Fig. 2c. Next, we constructed a model to represent the anionic polymer-coated antibody liquid, denoted as [C-IgG][S] in Fig. 2c. In this model, except for the six buried acidic residues, all other acidic residues were cationized from the reference structure (Supplementary Fig. 12c). The resulting C-IgG was neutralized by 252 anionic polymer surfactants (Supplementary Fig. 12d) and equilibrated at eight different temperatures (25:25:200 °C). After equilibration,

all the end-point structures at different temperatures show that the C-IgG is confined by a continuous polymer surfactant corona of [S] in the absence of free unbound polymer-surfactant molecules. An exemplary wrapping configuration is shown in Fig. 1c. In these structures, conjugation and wrapping do not seem to affect the antibody secondary structure. From the total 16 simulations, we determined the change in secondary structure (β -sheet, turns & coils) of IgG or [C-IgG][S] at each temperature as a means to measure unfolding of antibody structure. When the temperature is higher than 75 °C, the secondary structure of IgG in water undergoes significant structural changes as shown in Fig. 2c. In contrast, the secondary structure of [C-IgG][S] remains stable up to 200 °C and is consistent with the thermal stability of

lysozyme at 200 °C²². This stability is also in agreement with our experimental binding observations by QCM and structural analysis of the amide I region by FTIR after heating to 200 °C (Supplementary Fig. 13). In parallel, we also experimentally measured the secondary structures of IgG and [C-IgG][S] vs temperature. To replicate the conditions used for simulations, we used CD and FTIR spectroscopy to measure changes in the secondary structures of aqueous IgG and water-free [C-IgG][S] upon heating (Supplementary Fig. 14). However, it should be noted that the absolute values of secondary structure content differed between measurement techniques and deconvolution methods. This is an expected outcome given that FTIR is more reliable at predicting β -sheets and CD is better at estimating α -helices⁴⁶. Heating of aqueous IgG showed a loss in β -sheet content and an increase in the number of turns after deconvolution of CD peaks; while peak fitting of the broad amide I band of [C-IgG][S] at $\sim 1640\text{ cm}^{-1}$ showed minor changes in β -sheet, turns, and coil content upon heating (Supplementary Fig. 14). By comparison, there was a high degree of correlation between experimentally and computationally determined trends in secondary structure vs heating (Fig. 2c). In the case of [C-IgG][S], confinement by the polymer shell was primarily responsible for the extreme thermal stability as also observed by other groups for different solvent-free protein liquids^{29,47}.

Creation and characterization of water-free antibody liquid-based plastic materials.

Besides exhibiting thermal stability, solvent-free protein liquids have also been shown to display unconventional solubility properties in organic solvents and anhydrous ionic liquids that deviate from natural proteins^{26,33,48–52}. Generally, natural proteins possess an inability to function and operate in non-physiological and harsh environmental conditions (organic solvents, high temperatures) because of poor solubility, denaturation, and aggregation^{53,54}. However, the ability to access the biological activity of proteins in organic solvents, anhydrous ionic liquids, and/or in biologically incompatible materials (e.g., plastics) is an appealing property that presents new opportunities for biomolecules. For example, solvent-free protein liquids of M13 bacteriophage, glucosidase, and α -chymotrypsin showed enhanced solubility and thermal stability in anhydrous ionic liquids^{33,49–51} while in another example, peroxidase and hydrolase enzymes wrapped with random heteropolymers demonstrated increased solubility and stability in toluene⁵⁵. Similarly, we examined the universal solubility, high-temperature processibility, and compatibility of [C-IgG][S] with inert high molecular weight polymeric plastics to create bioactive thermoplastics with biorecognition capability. To demonstrate universal solubility of [C-IgG][S], we reconstituted [C-IgG][S] or rabbit IgG powder in water, toluene, chloroform, and acetone (Fig. 3a). In all, the lyophilized IgG powder was only soluble in water; while [C-IgG][S] was soluble in all solvents tested.

Next, we selected a hot melt adhesive (e.g., hot glue sticks) from a large set of commercial plastics because of its high viscosity when melted as well as multiple uses and applications. Because of the general incompatibility with biological materials (e.g., insolubility in water and high melting temperature), hot glue represents a challenging and non-traditional thermoplastic for the incorporation of antibodies. Initially, we created a simple version of hot glue by combining poly(ethylene-co-vinyl acetate), glycerol ester of gum rosin, and paraffin wax in a 2:1:1 wt ratio. The labmade hot glue exhibited comparable melting, viscosity, adhesion, and consistency to commercial-grade products (SurbonderTM cool shot mini glue sticks) (Supplementary Fig. 15). For processing antibodies with plastic, we melted a piece of commercial hot glue (mp = $\sim 90\text{ }^\circ\text{C}$) in the presence of cationized

goat anti-rabbit IgG conjugated to 15 nm Au particles with [S] to yield [C-GAR-Au][S], [C-IgG][S] from rabbit serum, or [anti-ferritin C-IgG][S] ($\sim 10\text{ wt}\%$) on a hot plate at $\sim 140\text{ }^\circ\text{C}$ until flowing, blended both materials together to reach homogeneity, and solidified into the new material by cooling (Supplementary Fig. 16). The glue blended antibody materials were remelted and molded in the shape of a rectangular block and arbitrary forms using appropriate PDMS molds to produce desired shapes (Fig. 3). As a control, we also blended hot glue with lyophilized rabbit IgG powder (unmodified) at $\sim 10\text{ wt}\%$ and observed the presence of clumps due to incompatibility (Supplementary Fig. 17). To show the uniformity of antibody liquids in glue, we exploited the optical properties of [C-GAR-Au][S] to create red rectangular blocks (Fig. 3b). By UV-Vis, the plasmon resonance of gold nanoparticles from [C-GAR-Au][S] in glue showed similar peak shapes and wavelengths to unmodified GAR-Au in water (Fig. 3b); while EDAX mapping of the cross-sectioned rectangular block pieces showed the presence of evenly distributed gold signals (Supplementary Fig. 18). Also, the cross-sectioned blocks of [C-GAR-Au][S]/glue showed no leaching of the gold-antibody conjugate after 5 days in water, thus confirming that the gold-antibody conjugate is physically entrapped inside the polymeric hot glue.

Moreover, we examined the binding ability of [C-IgG][S] in hot glue. To date, surface binding on plastics is achieved by simple adsorption processes or conventional surface immobilization techniques of biomolecules on polypropylene via standard functionalization/coupling chemistries⁵⁶. However, beyond surface functionalization of plastics, the poor compatibility of natural proteins has prevented successful integration/blending with plastics without the use of methylene diphenyl diisocyanate for soy protein isolate⁵⁷ or silica encapsulation of DNA to facilitate increased miscibility with polycaprolactone⁵⁸. In a similar example, partially shielded enzymes buried in silica were shown to exhibit enhanced tryptic activity with large protein substrates⁵⁹. After processing and molding, [C-IgG][S] or lyophilized rabbit IgG powder embedded in hot glue was assayed for binding and homogeneity by incubating antibody/hot glue molds with secondary antibodies raised against rabbit IgG (Goat Anti-Rabbit conjugated with alkaline phosphatase GAR-AP) or horse radish peroxidase (GAR-HRP)). As a result, the molded forms of [C-IgG][S]/hot glue showed binding of GAR-AP over its entire surface upon addition of the colorimetric substrate; while hot glue only remained colorless (Fig. 3c). Binding of the secondary antibody to the plastic confirms that the Fc regions of [C-IgG][S] embedded within the hot glue polymer are accessible to large macromolecules. By comparison, the lyophilized antibody powder blended with hot glue showed a lack of binding to GAR-HRP by chemiluminescence (Supplementary Fig. 19) and an absence of silver staining compared to [C-IgG][S] in glue (Supplementary Fig. 20).

To determine the presence and binding activity of [C-IgG][S] throughout the hot glue, we cross-sectioned the glue stick only and molded bioplastic materials and measured binding using GAR-HRP antibodies. In the cross-sectioned plastic materials, the HRP-conjugated antibodies should only bind to the interior area of the new unexposed glue given that the IgG antibodies near the glue surface were already blocked by bound GAR-AP antibody conjugates. As expected, only the cross-sectioned plastic pieces containing [C-IgG][S] showed a chemiluminescence signal indicative of binding to GAR-HRP (Fig. 3c). In total, these results confirm that the [C-IgG][S] liquid is uniformly blended throughout the entire hot glue material and biologically active. To achieve miscibility with plastic, [C-IgG][S] features an amphiphilic wrapping polymer that contains a hydrophilic and hydrophobic region. In these materials, the charged hydrophilic

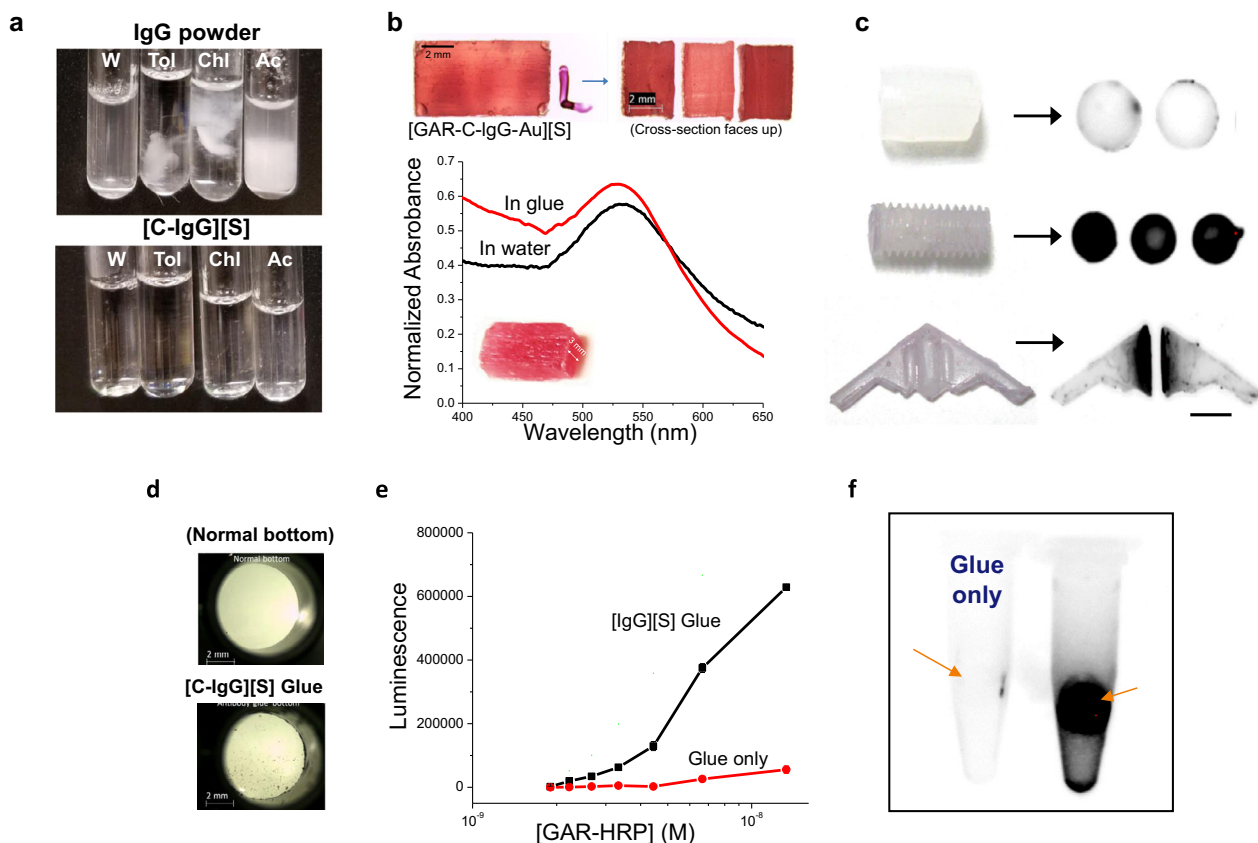


Fig. 3 Creation of bioplastic containing IgG liquids in hot glue. **a** Solubility of IgG powder (control) or [C-IgG][S] in water (W), toluene (Tol), Chloroform (Chl), and acetone (Ac). **b** Top view image of hot glue blended with [GAR-C-IgG-Au][S], molded into a single rectangular block, and then cross-sectioned into three pieces (illuminated from below on a glass slide with AFRL written). The three red block pieces are shown with cross-sectioned area facing upward and bottom illumination. UV-Vis plot of [GAR-C-IgG-Au][S] in glue or GAR-IgG-Au in water. Inset shows block dimensions. **c** Colorimetric assay of hot glue cylinder (control) and molded forms of [C-IgG][S]/glue after incubation with GAR-AP and addition of colorimetric substrate (Left column). Chemiluminescence of the cross-sectioned hot glue cylinder (control) and cross-sectioned forms of [C-IgG][S]/glue after incubation with GAR-HRP and addition of chemiluminescent substrate (Right column). Scale bar equals 6 mm. **d** Images of well bottoms from a 96-well plate with a normal surface or with the bottom replaced with [C-IgG][S] glue. **e** Binding assay of antibody glued well bottoms with multiple concentrations of GAR-HRP. Chemiluminescence was measured for each well using a microplate reader. Error bars represent standard deviation from triplicate measurements. **f** Sandwich binding assay of [anti-ferritin C-IgG][S] in glue with apoferritin and anti-ferritin antibody conjugated to HRP. Image shows chemiluminescence of control and antibody glue with arrows indicating location of glue pieces in tube.

end of the anionic polymer interacts directly with the cationized antibody surface, while the hydrophobic tail is exposed to the hydrophobic environment of high molecular weight poly(ethylene-co-vinyl acetate) polymers or organic solvents. Because of these favorable hydrophobic interactions, the miscibility of [C-IgG][S] with melted hot glue was significantly increased. ATR-FTIR of antibody glue revealed a shifted peak associated with the H-C-O bending modes of vinyl acetate (Supplementary Fig. 21)⁶⁰. This suggests [C-IgG][S] interacts primarily with the vinyl acetate region of poly(ethylene-co-vinyl acetate) in hot glue. In addition, the amide I region of [C-IgG][S] in glue showed an increase in β -sheet structure relative to the water-free [C-IgG][S] material only due to the hydrophobic nature of hot glue.

We exploited the adhesive properties of antibody glue to join two pieces of a microfuge tube together. In this application, the glued microfuge pieces produced a water-tight seal; while at the same time, imparted antigen binding to the glued interface by containing embedded [C-IgG][S] (Supplementary Fig. 22). To assess activity, GAR-HRP antibodies were added to the glued tube and incubated to promote binding. After binding and washing, addition of luminol/peroxide produced a chemiluminescent signal localized to the glued interface (Supplementary Fig. 22).

Similarly, we replaced the well bottoms of a conventional 96-well plate with antibody glued bottoms (Fig. 3d). To construct well bottoms with glue, we punched out the existing plastic surfaces of wells, pressed and molded melted antibody glue over wells to form a water-tight seal, and then cooled glue to form solid bottoms. In this 96-well format, a microplate reader was used to measure the surface binding of antibody glued wells. For binding measurements, we incubated the set of glued wells with different concentrations of GAR-HRP, washed, and measured chemiluminescence according to ELISA protocols. Consequently, we obtained an exponential increase in chemiluminescence for antibody glued wells upon increasing concentration of secondary antibody (Fig. 3e) and only a slight increase in fluorescence for glued bottoms only. In a final example, we replaced the liquid form of [C-IgG][S] from rabbit serum displaying broad binding specificity with an antigen-specific primary antibody [anti-ferritin C-IgG][S] to determine the binding range of antibodies in hot glue. [anti-ferritin C-IgG][S] liquid blended with hot glue or hot glue only (no antibodies) were incubated with apoferritin antigen, washed, and then interrogated with anti-ferritin antibodies conjugated with HRP in a sandwich assay format. Addition of luminol/H₂O₂ produced a strong chemiluminescent signal for the

antibody glue indicative of apoferritin binding to the antibody/glue surface (Fig. 3f). In all, we have tested the F_C and F_V regions of an antibody embedded in hot glue for binding and demonstrated that both regions remain functional for binding.

Conclusion. In total, we converted thermally labile primary IgG antibodies into stable water-free antibody liquids. For example, [anti-ferritin C-IgG][S] retained >60% binding activity after repeated heating cycles up to 125 °C and displayed partial binding even after heating to 200 °C. This represents a significant improvement over other stabilization methods for antibodies that include encapsulation, immobilization, and/or use of stabilizing excipients. In addition, we expect this process to be broadly applicable to all antibody isotypes (IgM, IgY, IgG) and impart similar stabilization at high temperatures; however, optimization will be needed for each isotype. In a separate and parallel study, evaluation of the therapeutic potential of antibody liquids revealed cytotoxicity at high concentrations against several common cell lines⁶¹. Consequently, antibody liquids will require improvements in their design and/or replacement of stabilizing anions in order to be suitable for therapeutic applications.

For diagnostics, we exploited the thermal stability, universal solubility, and material compatibility properties of antibody liquids to create bioactive antibody plastics and glues using high molecular weight hot melt adhesives. Notably, antibody embedded plastics are in a “ready to use” bioactive format and do not require removal of proteins/biomolecules from plastic unlike DNA stored in polycaprolactone. As described above, DNA encapsulated in SiO₂ and dispersed in polycaprolactone requires extraction by tetrahydrofuran and purification for utilization. Also, the high loading and homogenous blend of antibodies embedded throughout plastic offer the ability to harness, replicate, and access biological activity from anywhere within a plastic structure by cross-sectioning into multiple pieces and/or remolding into new forms to generate a renewable surface. The ability to generate renewable bioactive surfaces on demand is advantageous for the manufacturing of multi-use diagnostics vs. single-use disposable devices, lateral flow assays, and responsive packaging that is capable of sensing antigens or pathogens. In addition, we envision antibody-embedded plastics for use in crack detection, whereby damage to the plastic surface would result in the exposure of active antibodies as demonstrated above.

Methods

Synthesis of water-free antibody liquid. For antibody cationization, 100 μ L of polyclonal anti-horse spleen ferritin antibody (anti-ferritin IgG) (1 mg/mL stock, Sigma) and 20 μ L of 3-dimethylaminopropylamine (Sigma-Aldrich) adjusted to a pH of 5–6 was added to 1 mL of 0.1 M MES buffer pH 5.0 in a 2 mL microfuge tube. 0.25 mg of EDC (1-ethyl-3-(3-dimethylaminopropyl) carbodiimide hydrochloride, Sigma-Aldrich) was added to antibody and cationizing agent to induce coupling. The coupling reaction was incubated for 2 h at room temperature and then dialyzed in a slide-A-Lyzer dialysis cassette (3500 MWCO 3 mL volume) (Thermo Fisher) at 4 °C in water for 2 days to remove salts and excess coupling reagents. Over 2 days of dialysis, the water was changed 4–5 times. After dialysis, the cationized antibody (C-IgG) product was centrifuged at 14,000 rpm for 2 min to remove any cross-linked and/or precipitated antibody. The antibody liquid was prepared by adding 0.3 mg of Poly(ethylene glycol) 4-nonylphenyl 3-sulfopropyl ether potassium salt [S] (Sigma-Aldrich) dissolved in 100 μ L of doubly deionized water to the dialyzed C-IgG to balance charges and incubated for 1 h on a rocker at room temperature. After 1 h, the [C-IgG][S] complex was again dialyzed to remove excess anion of [S] using 3500 MWCO dialysis cartridges. [anti-ferritin C-IgG][S] was frozen at –80 °C for 10 min and lyophilized on a Labconco freeze dry system for 18 h to complete dryness. After lyophilization, [C-IgG][S] was melted by gently warming lyophilized powder to ~45 °C on a hot plate to form a viscous antibody liquid.

Characterization. Zeta potential and dynamic light scattering (DLS) measurements were obtained on a Malvern nano series Zetasizer using a disposable folded capillary cell (Malvern, DTS1070) or 1 mL disposable cuvette. For zeta potential measurements, 0.1 mg of rabbit IgG, [C-IgG][S], or anion of [S] only were

dissolved in 600 μ L of deionized water. Thermal properties were measured on a TA Instruments Discovery series DSC 2500. Samples were weighed, transferred to an aluminum pan, and sealed with lid. Samples were equilibrated at –40 °C and then heated to 200 °C with a heating ramp of 5 °C per minute. Samples were then cooled to –40 °C at 5 °C per minute. Heating/cooling was cycled 2 more times. Circular dichroism spectra were collected on a Jasco J-815 CD spectrometer using a quartz cuvette with a 1 cm pathlength from 260 to 190 nm at a scan rate of 20 nm/min and averaged over 3 repetitive scans. Temperature studies were performed using a Peltier controlled cuvette holder from 25 to 100 °C at 25 °C increments. Samples were equilibrated at each temperature for 10 min before scanning. CD spectra were analyzed for secondary structure content using CDPro software. FTIR spectra were collected using a Bruker Lumos II FTIR microscope in reflection or attenuated total reflectance (ATR) modes. Samples were prepared by smearing ~1 μ L of water-free [C-IgG][S] and [S] only onto a gold-coated polished silicon wafer (Wafer World). Initially, a background scan of [S] only averaged over 64 scans was performed and automatically subtracted from FTIR measurements of [C-IgG][S] to remove strong vibrational modes associated with [S]. Heating experiments were performed in situ by using a heated microscope stage with temperature control. Secondary structure content was determined by finding the second derivative of broad Amide I band (~1645 cm⁻¹), assigning peaks to known secondary structures, fitting peaks using gaussian multiple peak fitting function, and integrating the area of each peak using Origin Pro software (v. 6.1)⁶².

Ouchterlony double diffusion gels. Multiple pattern immunodiffusion plates with agarose gelling agent (Thermo Scientific, product #31111) were used to detect antibody-antigen binding and determine antigen identity. In the center well, we pipetted 20 μ L of 125 μ g of apoferritin (25 mg/mL stock, Sigma) in water. To the 6 surrounding wells, we pipetted 7 μ L of anti-ferritin IgG antibody (1 mg/mL stock, Sigma) in duplicate alternating wells, 7 μ L of anti-ferritin C-IgG (1 mg/mL) only, 7 μ L of anti-ferritin C-IgG (1 mg/mL) with 28 μ L of [S] poly(ethylene glycol) 4-nonylphenyl 3-sulfopropyl ether potassium salt (1 mg/mL in water, Sigma-Aldrich) lyophilized and, 7 μ L of anti-ferritin IgG (1 mg/mL stock, Sigma) with 28 μ L of [S] poly(ethylene glycol) 4-nonylphenyl 3-sulfopropyl ether potassium salt (1 mg/mL in water, Sigma-Aldrich), and 28 μ L of [S] poly(ethylene glycol) 4-nonylphenyl 3-sulfopropyl ether potassium salt (1 mg/mL in water, Sigma-Aldrich) only. Immunodiffusion plates loaded with samples were incubated for 18 h at room temperature to promote immunoprecipitation. After 18 h, the plates were stained in order to better visualize immunoprecipitation lines. Gels were carefully cut out and soaked in water for 30 min, pressed dry by weighting it under 3 pieces of blotting paper for 20 min, soaked in 0.9% sodium chloride for 30 min, pressed dry for 20 min with weighted blotting paper, and repeated 3 more times. Finally, the gel was dried using low heat setting on a hair drier (1000 W). The dried gel was stained in coomassie stain for 15 min and destained in 10% acetic acid for ~8 h.

Thermal stability measurements. 1 mg of [anti-ferritin C-IgG][S] kept at 25 °C for 30 min was reconstituted in 1 mL of double deionized water to yield a concentration of 1 mg/mL in a microfuge tube. For binding measurements, 10 μ L of the reconstituted [anti-ferritin C-IgG][S] (1 mg/mL) was diluted in 20 mL of water. The remaining 990 μ L of antibody liquid was frozen at –80 °C for 10 min and lyophilized to dryness. The lyophilized water-free antibody liquid was then heated at 50 °C in a Benchmark myblock™ mini dry bath for 30 min, cooled to room temperature for 10 min, reconstituted in 990 μ L of deionized water to yield 1 mg/mL, and diluted at 1:2000 by adding 10 μ L of antibody liquid in 20 mL of water for binding measurements. The reconstituted antibody liquid was then frozen at –80 °C and lyophilized to dryness. The lyophilized antibody liquid was subsequently heated to 75 °C, cooled, reconstituted at 1 mg/mL, diluted at 1:2000, refrozen, lyophilized, and heated at the next temperature of 100 °C. This was repeated for 125 °C.

QCM measurement of binding activity. A Q-Sense E4 quartz crystal microbalance with dissipation (QCM-D) was used to measure antibody binding to an immobilized antigen. Gold-coated QCM sensors (QuartzPro) were cleaned via UV-ozone treatment for 10 min, followed by heating in a 7.5:1:1 solution of water/30% H₂O₂/NH₄OH at 80 °C for 10 min, thorough rinsing with double deionized water, and dried with N₂. The cleaned gold-coated sensors were mounted in a Q-Sense flow cell module. To test antibody binding, antigens of apoferritin was first immobilized on gold-coated QCM sensors in situ by flowing apoferritin (75 μ L of 25 mg/mL apoferritin stock in 10 mL water) at a flow rate of 0.17 mL/min across gold surface until binding curve showed saturation (~15 min). After surface was saturated with apoferritin, the surface was washed for at least 20 min by flowing water. For Antibody binding, antibody liquids were reconstituted in water to yield a 1 mg/mL concentration and then further diluted by adding 10 μ L of reconstituted antibody liquid (1 mg/mL) in 20 mL of double deionized water to yield a 1:2000 dilution. For all measurements, a flow rate of 0.17 mL/min and a constant temperature controlled at 23 °C was used; while the 3rd overtone resonance frequency was monitored and used to calculate % antigen binding and equilibrium binding constants. To calculate % antigen binding, the raw frequency plots were converted to an aerial mass (ng/cm²) using the Sauerbrey equation. The masses of adsorbed

apoferritin after saturation of the QCM surface and bound antibody after 1 h of binding were extrapolated from plots, converted into number of moles, and then used to determine a mole ratio of antibody/apoferritin at each temperature in triplicate. The mole ratio at 25 °C was used to represent 100% antigen binding for each antibody modification according to this equation, % binding = (mole ratio of antibody/apoferritin @ 25 °C)/(mole ratio of antibody/apoferritin @ 25 °C) × 100%. The frequency plots were then fit to a Langmuir binding isotherm and used to calculate equilibrium binding constants via known methods.

Immunoblot binding assay. For immunoblot, 200 µL of 10 pM, 100 pM, 1 nM, 100 nM, and 1 µM of apoferritin (Sigma) were spotted onto a 4 inch × 0.5 inch PVDF membrane with 0.45 µm pore size (Invitrogen) using a Biorad immunoblotting well plate. The entire membrane was then blocked by immersion in ~5 mL of tris buffered saline with 0.1% tween 20 (TBST) and 1% non-fat powdered milk in a sterile petri dish for 2 h. In this case, blocking with milk generally produces a lower background signal with polyclonal antibodies as compared to BSA. During this time, the membrane was gently agitated on a rocker. After blocking, TBST with 1% milk was removed and replaced with antibody liquid reconstituted in TBST/milk (20 µg dissolved in 3 mL TBST with 1% milk). The antibody liquid of [anti-ferritin C-IgG][S] or control anti-ferritin IgG antibody was incubated with immobilized apoferritin protein on membrane for 4 h and agitated on a rocker. After 4 h, the reconstituted antibody liquid in TBST with 1% milk was removed from membrane, and 5 mL of fresh TBST with 1% milk was added in order to wash excess unbound antibody. The membrane was washed 2 more times with fresh TBST with 1% milk. After a total of 3 wash steps, a goat anti-rabbit secondary antibody conjugated with alkaline phosphatase was added to membrane at 1:1000 dilution in TBST with 1% milk and incubated for 4 h. After 4 h, the membrane was again repeatedly washed 3 times with 5 mL of TBST and 1 time with double deionized water. Finally, these binding interactions were detected colorimetrically by exposing membrane to 3 mL of substrate (nitroblue tetrazolium/5-bromo-4-chloro-3-indolyl phosphate) for 5 min. After 5 min, the membranes were extensively washed with double deionized water and a digital image was recorded using a point and shoot 12 MP Canon digital camera.

Creation of antibody liquid/hot glue plastics. 0.2 g of poly(ethylene-co-vinyl acetate) with 12% vinyl acetate (Sigma-Aldrich, product #437247) was combined with 0.1 g of paraffin wax (Sigma-Aldrich, product #) and 0.1 g of glycerol ester of pine rosin (Chemical Store, product code ESTERGL90). The mixture was heated at 170 °C on a hot plate until melted and then vigorously blended together until homogeneity was reached. For incorporation of antibodies, 1–10 wt% antibody liquid comprised of [goat anti-rabbit C-IgG conjugated to 15 nm Au particles][S] (BBI International), [C-IgG][S], or [anti-ferritin C-IgG][S] was thoroughly blended on a hot plate with melted hot glue at 140 °C on a glass slide using a metal spatula. The blended material was cooled to room temperature and then removed from the glass slide using a razor blade as a rough sheet. The antibody glue was then molded into desired shapes using PDMS molds (Dow Corning Sylgard-184) prepared from a 1:1260 scale B2 bomber replica, rectangular block, cylinder, and a threaded screw by packing solid glue pieces in molds and remelting in a vacuum oven at ~125 °C for 10 min. The molded antibody glue structures were cooled to room temperature and allowed to solidify for 20 min before removing from molds. The rabbit IgG antibody glue structures or glue only pieces were assayed for binding by incubating with a goat anti-rabbit HRP conjugate (Bio-Rad, 2 mg/mL, 1:2000) or a goat anti-rabbit alkaline phosphatase conjugate (Bio-Rad, 2 mg/mL, 1:2000) in TBS buffer with 0.1% tween (TBST) and 1% non-fat dry milk for 2 h with gentle rocking. After 2 h, the glue structures were washed with TBST and milk 3x followed by washing with water 2x. After washing, glue structures were incubated with 1–3 mL of SuperSignal West Pico PLUS chemiluminescent substrate and imaged on a Bio-Rad ChemiDoc MP Imaging System. Glue containing [anti-ferritin C-IgG][S] or glue only was incubated with 2 nM apoferritin (Sigma) in TBST with milk for 2 h and washed 3x with TBST milk. After washing, glue samples were incubated with an anti-ferritin antibody conjugated to HRP at 1:2000 dilution in TBST milk for 2 h. Anti-ferritin antibodies were conjugated with HRP using an HRP conjugation kit (Abcam, ab102890). Glue samples were washed with TBST milk 3 times and water 2 times. SuperSignal West Pico PLUS chemiluminescent substrate was added to sample glue pieces in a microfuge tube and imaged. Polystyrene black 96-well plates with clear flat bottoms (Corning) were modified by first removing well bottoms using a biopsy hole punch. The openings of the well holes were then smoothed using a metal file and glued using [C-IgG][S] glue or hot glue only. To glue bottoms of well plate, [C-IgG][S] glue was melted and smeared onto a piece of Al foil. The foil with melted glue was firmly pressed onto backside of well plate and cooled. The glued bottoms were checked for leaks by placing 200 µL of water into each well and then assayed for binding. For binding, 200 µL of GAR-HRP at dilutions of 1:7000, 1:6000, 1:5000, 1:4000, 1:3000, 1:2000, 1:1000 in TBST/milk were incubated in the set of glued wells for 2 h, washed 3x, and measured for chemiluminescence by addition of 200 µL of Pico PLUS substrate on a BioTek Synergy neo2 multi-mode reader.

Molecular dynamics simulation. All MD simulations were performed using the NAMD 10b2⁶³. The CHARMM general force field V4.1 and CHARMM36

all-hydrogen parameter file for proteins were used. The starting IgG structure was taken from the Protein Data Bank (pdb access code 1hzh). This crystal structure has a resolution of 2.7 angstrom. This protein consists of 4 chains: two heavy chains H and K, and two light chains. Each heavy chain has 457 residues. Each light chain has 215 residues. Using VMD 1.9.2 software⁶⁴, the protein was solvated in a cuboid of 70655 TIP3 water molecules and 22 chloride ions for neutralization of the system. The system was first minimized and heating up to 298.15 K. Then 500 ps equilibrations were carried out in NVT ensemble before 200 ns equilibration were carried out in NPT ensemble. The end-point structure was used as the starting structure for further simulations of two different models. One model involves IgG without modification in a generalized Born implicit water model, denoted by IgG. Starting with the pre-equilibrated IgG after 200 ns MD simulations in explicit water as indicated in Supplementary Fig. 12a and f, three independent MD simulations with different initial velocities were performed for another 200 ns for each temperature using the generalized Born implicit water model to save computational time. The solvent dielectric constant was set 78.5 to represent water effect. The time evolution of the radius of gyration of protein is shown in Supplementary Fig. 23a-c.

The other model involves unburied acidic residues that were cationized [C-IgG] and then neutralized by anionic polymer surfactants [S], denoted by [C-IgG][S]. We first constructed the [C-IgG][S] model to represent the anionic polymer-coated [C-IgG][S] liquid and pre-equilibrated in vacuum for 200 ns as indicated in Supplementary Fig. 12c, d and f. The vacuum dielectric constant 1 was chosen to guarantee no modification of the electrostatic interactions between C-IgG and the anionic polymer surfactants which replace water. Restarting the MD simulations with three different snapshots from the pre-equilibrated trajectory, three independent MD simulations were carried out for a simulation period ranging from 30 to 260 ns for 8 independent simulations at 8 different temperatures with dielectric constant 1. The time evolution of the radius of gyration of protein is shown in Supplementary Fig. 23d-f. In both cases, the last 50 snapshots recorded every 0.05 ns in each trajectory were used to estimate the average secondary structure contents and their error bars using VMD⁶⁴. In the TIP3 water model simulation, Particle mesh Ewald summation was employed to account for long-range electrostatics and a 12 Å cutoff for the van der Waals interaction was implemented. The pressure was maintained at 1 atm using Langevin piston. In the generalized Born solvent model simulation, cutoff 32.0 Å, switchdist 30.0 Å, pairlistdist 36.0 Å, and alphaCutoff 14.0 Å were implemented. In the anionic polymer surfactant model, no water was included because the anionic polymer surfactant acted as the solvent. The system is in a dielectric medium. A cutoff 24 Å was used for calculating both van der Waals and electrostatics interactions.

Data availability

The authors declare that the data supporting the findings of this study are available within the paper and its supplementary information files.

Received: 31 May 2021; Accepted: 26 November 2021;

Published online: 20 December 2021

References

1. Wang, C. et al. Ultrarobust biochips with metal-organic framework coating for point-of-care diagnosis. *ACS Sensors* **3**, 342–351 (2018).
2. Wang, C. et al. Metal-organic framework encapsulation for biospecimen preservation. *Chem. Mater.* **30**, 1291–1300 (2018).
3. North, J. R. Immunosensors: antibody-based biosensors. *Trends Biotechnol.* **3**, 180–186 (1985).
4. Byrne, B., Stack, E., Gilmartin, N. & O’Kennedy, R. O. Antibody-based sensors: principles, problems, and potential for detection of pathogens and associated toxins. *Sensors* **9**, 4407–4445 (2009).
5. Holford, T. R. J., Davis, F. & Higson, S. P. J. Recent trends in antibody based sensors. *Biosensors Bioelectron.* **34**, 12–24 (2012).
6. Borrebaeck, C. A. K. Antibodies in diagnostics- from immunoassays to protein chips. *Immun. Today* **21**, 379–382 (2000).
7. Johnson, M. Antibody storage and antibody shelf-life. *Mater. Methods.* **2**, 120 (2012).
8. Wang, C. et al. Metal-organic framework as a protective coating for biodiagnostic chips. *Adv. Mater.* **29**, 1604433 (2017).
9. Guziewicz, N. A., Massetti, A. J., Perez-Ramirez, B. J. & Kaplan, D. L. Mechanisms of monoclonal antibody stabilization and release from silk biomaterials. *Biomater.* **34**, 7766–7775 (2013).
10. Li, A. B., Kluge, J. A., Guziewicz, N. A., Omenetto, F. G. & Kaplan, D. L. Silk-based stabilization of biomacromolecules. *J. Controlled Release* **219**, 416–430 (2015).
11. Wang, C. et al. Silk-encapsulated plasmonic biochips with enhanced thermal stability. *ACS Appl. Mater. Inter.* **8**, 26493–26500 (2016).

12. Park, J.-W. et al. Comparison of stabilizing effect of stabilizers for immobilized antibodies on QCM immunosensors. *Sens. Actuat. B:Chem.* **91**, 158–162 (2003).
13. Comert, F., Malanowski, A. J., Azarikia, F. & Dubin, P. L. Coacervation and precipitation in polysaccharide-protein systems. *Soft Matt.* **12**, 4154–4161 (2016).
14. Blocher McTigue, W. C. & Perry, S. L. Design rules for encapsulating proteins into complex coacervates. *Soft Matt.* **15**, 2089–3103 (2019).
15. Harmsen, M. M. & De Haard, H. J. Properties, production, and applications of camelid single-domain antibody fragments. *Appl. Microbiol. Biotechnol.* **77**, 13–22 (2007).
16. Hu, R., Luan, J., Kharasch, E. D., Singamaneni, S. & Morrissey, J. J. Aromatic functionality of target proteins influences monomer selection for creating artificial antibodies on plasmonic biosensors. *ACS Appl. Mater. Interf.* **9**, 145–151 (2017).
17. Schiro, G. et al. Diffusivelike motions in a solvent-free protein-polymer hybrid. *Phys. Rev. Lett.* **126**, 088102 (2021).
18. Gallat, F. X. et al. A polymer surfactant corona dynamically replaces water in solvent-free protein liquids and ensures macromolecular flexibility and activity. *J. Am. Chem. Soc.* **134**, 13168–13171 (2012).
19. Liu, K., Ma, C., Gostl, R., Zhang, L. & Herrmann, A. Liquefaction of biopolymers: solvent-free liquids and liquid crystals from nucleic acids and proteins. *Acc. Chem. Res.* **50**, 1212–1221 (2017).
20. Perriman, A. W., Colfen, H., Hughes, R. W., Barrie, C. L. & Mann, S. Solvent-free protein liquids and liquid crystals. *Angew. Chem. Int. Ed.* **48**, 6242–6246 (2009).
21. Perriman, A. W. & Mann, S. Liquid proteins—a new frontier for biomolecule-based nanoscience. *ACS Nano* **8**, 6085–6091 (2011).
22. Brogan, A. P. S., Sharma, K. P., Perriman, A. W. & Mann, S. Isolation of a highly reactive beat-sheet-rich intermediate of lysozyme in a solvent-free liquid phase. *J. Phys. Chem. B* **117**, 8400–8407 (2013).
23. Sharma, K. P. et al. Self-organization of glucose oxidase-polymer surfactant nanoconstructs in solvent-free soft solids and liquids. *J. Phys. Chem. B* **118**, 11573–11580 (2014).
24. Brogan, A. P. S., Sharma, K. P., Perriman, A. W. & Mann, S. Enzyme activity in liquid lipase melts as a step towards solvent-free biology at 150 degrees C. *Nat. Commun.* **5**, 5058 (2014).
25. Perriman, A. W. et al. Reversible dioxygen binding in solvent-free liquid myoglobin. *Nat. Chem.* **2**, 622–626 (2010).
26. Mukhopadhyay, A., Das, T., Datta, A. & Sharma, K. P. Neat Protein-polymer surfactant bioconjugates as universal solvents. *Biomacromol.* **19**, 943–950 (2018).
27. Liu, K. et al. Solvent-free liquid crystals and liquids from. *DNA. Chem.-A European J.* **21**, 4898–4903 (2015).
28. Patil, A. J. et al. Liquid viruses by nanoscale engineering of capsid surfaces. *Adv. Mater.* **24**, 4557–4563 (2012).
29. Bui-Le, L., Brogan, A. P. S. & Hallett, J. P. Solvent-free liquid avidin as a step toward cold chain elimination. *Biotechnol. Bioengin.* **118**, 592–600 (2020).
30. Atkins, D. L., Berrocal, J. A., Mason, A. F. & Voets, I. K. Tandem catalysis in multicomponent solvent-free biofluids. *Nanoscale* **11**, 19797–19805 (2019).
31. Zhang, W. H. et al. Sequential electrostatic assembly of a polymer surfactant corona increases activity of the phosphotriesterase arPTE. *Bioconjug. Chem.* **30**, 2771–2776 (2019).
32. Atkins, D. L., Magana, R., Sproncken, C. C. M., van Hest, J. C. M. & Voets, I. K. Single enzyme nanoparticles with improved biocatalytic activity through protein entrapment in a surfactant shell. *Biomacromolecules* **22**, 1159–1166 (2021).
33. Brogan, A. P. S., Heldman, N., Hallett, J. P. & Belcher, A. M. Thermally robust solvent-free biofluids of M13 bacteriophage engineered for high compatibility with anhydrous ionic liquids. *Chem. Commun.* **55**, 10752–10755 (2019).
34. Slocik, J. M., Dennis, P. B. & Naik, R. R. *Ultra-Stable Protein Ionic Liquids*. US patent #10,462,733 (2019).
35. Bartczak, D. & Kanaras, A. G. Preparation of peptide-functionalized gold nanoparticles using one pot EDC/sulfo-NHS coupling. *Langmuir* **27**, 10119–10123 (2011).
36. Thompson, D. B., Cronican, J. J. & Liu, D. R. Engineering and identifying supercharged proteins for macromolecule delivery into mammalian cells. in *Meth. Enzymol.*, 503 (Elsevier, 2012).
37. Rayner, L. E. et al. The solution structure of Rabbit IgG accounts for its interaction with the Fc receptor and complement C1q and its conformational stability. *J. Molec. Biol.* **425**, 506–523 (2013).
38. Rayner, L. E. et al. The solution structure of rabbit IgG accounts for its interactions with the Fc receptor and complement C1q and its conformational stability. *J. Molec. Biol.* **425**, 506–523 (2013).
39. Saphire, E. O. et al. Crystal structure of a neutralizing human IGG against HIV-1: a template for vaccine design. *Science* **293**, 1155–1159 (2001).
40. Joshi, V., Shivach, T., Yadav, N. & Rathore, A. S. Circular dichroism spectroscopy as a tool for monitoring aggregation in monoclonal antibody therapeutics. *Anal. Chem.* **86**, 11606–11613 (2014).
41. Zheng, K., Bantog, C. & Bayer, R. The impact of glycosylation on monoclonal antibody conformation and stability. *mAbs* **3**, 568–576 (2011).
42. Hornbeck, P. Double-diffusion assay for detecting specific antibodies (Ouchterlony). *Curr. Protoc. Immunol.* **116**, 2.3.1–2.3.4 (2017).
43. Bailey, G. S. *Ouchterlony Double Immunodiffusion* (Humana Press Inc., 1996).
44. Gerdon, A. E., Wright, D. W. & Cliffl, D. E. Quartz crystal microbalance detection of glutathione-protected nanoclusters using antibody recognition. *Anal. Chem.* **77**, 304–310 (2005).
45. Zhang, Y. & Rojas, O. J. Immunosensors for C-reactive protein based on ultrathin films of carboxylated cellulose nanofibrils. *Biomacromol.* **18**, 526–534 (2017).
46. Pribic, R., Vanstokkum, I. H. M., Chapman, D., Harris, P. I. & Bloemendal, M. Protein secondary structure from Fourier transform infrared and/or circular dichroism spectra. *Anal. Biochem.* **214**, 366–378 (1993).
47. Brogan, A. P. S., Siligardi, G., Hussain, R., Perriman, A. W. & Mann, S. Hyperthermal stability and unprecedented re-folding of solvent-free liquid myoglobin. *Chemical Science* **3**, 1839–1846 (2012).
48. Zhang, Y., Patil, A. J., Perriman, A. W. & Mann, S. Enhanced catalytic activity in organic solvents using molecularly dispersed haemoglobin-polymer surfactant constructs. *Chem. Commun.* **49**, 9561–9563 (2013).
49. Brogan, A. P. S. & Hallett, J. P. Solubilizing and stabilizing proteins in anhydrous ionic liquids through formation of protein-polymer surfactant nanoconstructs. *J. Am. Chem. Soc.* **138**, 4494–4501 (2016).
50. Mukhopadhyay, A., Singh, D. & Sharma, K. P. Neat ionic liquid and a-chymotrypsin-polymer surfactant conjugate-based biocatalytic solvent. *Biomacromol.* **21**, 867–877 (2020).
51. Brogan, A. P. S., Bui-Le, L. & Hallett, J. P. Non-aqueous homogenous biocatalytic conversion of polysaccharides in ionic liquids using chemically modified glucosidase. *Nat. Chem.* **10**, 859–865 (2018).
52. Patil, A. J. et al. Liquid viruses by nanoscale engineering of capsid surfaces. *Adv. Mater.* **24**, 4557–4563 (2012).
53. Houen, G. The solubility of proteins in organic solvents. *Acta Chem. Scand.* **50**, 68–70 (1996).
54. Chin, J. T., Wheeler, S. L. & Klibanov, A. M. On protein solubility in organic solvent. *Biotechnol. Bioengin.* **44**, 140–145 (1994).
55. Panganiban, B. et al. Random heteropolymers preserve protein function in foreign environments. *Science* **359**, 1239–1243 (2018).
56. Schiller, S. M. et al. “Plastic trash goes biohybrid”—Rapid and selective functionalization of inert plastic surfaces with biomolecules. *Macromol. Chem. Phys.* **211**, 222–228 (2010).
57. Zhong, Z. & Sun, X. S. Properties of soy protein isolate/polycaprolactone blends compatibilized by methylene diphenyl diisocyanate. *Polymer* **42**, 6961–6969 (2001).
58. Koch, J. et al. A DNA-of-things storage architecture to create materials with embedded memory. *Nat. Biotechnol.* **38**, 39–43 (2020).
59. Briand, M. L. et al. Partially shielded enzymes capable of processing large protein substrates. *Chem. Commun.* **56**, 5170–5173 (2020).
60. Ramirez-Hernandez, A., Aguilar-Flores, C. & Aparicio-Saguilan, A. Fingerprint analysis of FTIR spectra of polymers containing vinyl acetate. *DYNA* **86**, 198–205 (2019).
61. Nelson, M. T. et al. Examining cellular responses to reconstituted antibody protein liquids. *Sci. Rep.* **11**, 17066 (2021).
62. Yang, H., Yang, S., Kong, J., Dong, A. & Yu, S. Obtaining information about protein secondary structures in aqueous solution using Fourier transform IR spectroscopy. *Nat. Protoc.* **10**, 382–396 (2015).
63. Phillips, J. C. et al. Scalable molecular dynamics with NAMD. *J. Comp. Chem.* **26**, 1781–1802 (2005).
64. Humphrey, W., Dalke, A. & Schulten, K. VMD: visual molecular dynamics. *J. Molec. Graphics* **14**, 33–38 (1996).

Acknowledgements

The authors thank the Air Force Office of Scientific research for funding. P.B.D. is adjunct faculty at Wright State University, Department of Biochemistry and Molecular Biology.

Author contributions

J.M.S., P.B.D., and R.R.N. conceived idea, designed experiments, and wrote manuscript. J.M.S. performed synthesis, characterization, and binding experiments. Z.K. performed Molecular dynamics simulations and wrote the manuscript. A.P. performed differential scanning calorimetry measurements on materials.

Competing interests

J.M.S., P.B.D., and R.R.N. have received US patents (10,463,733 and 11,058,770). All other authors have no competing interests to declare.

Additional information

Supplementary information The online version contains supplementary material available at <https://doi.org/10.1038/s43246-021-00222-2>.

Correspondence and requests for materials should be addressed to Rajesh R. Naik.

Peer review information *Communications Materials* thanks the anonymous reviewers for their contribution to the peer review of this work. Primary Handling Editors: Rona Chandrawati and John Plummer.

Reprints and permission information is available at <http://www.nature.com/reprints>

Publisher's note Springer Nature remains neutral with regard to jurisdictional claims in published maps and institutional affiliations.



Open Access This article is licensed under a Creative Commons Attribution 4.0 International License, which permits use, sharing, adaptation, distribution and reproduction in any medium or format, as long as you give appropriate credit to the original author(s) and the source, provide a link to the Creative Commons license, and indicate if changes were made. The images or other third party material in this article are included in the article's Creative Commons license, unless indicated otherwise in a credit line to the material. If material is not included in the article's Creative Commons license and your intended use is not permitted by statutory regulation or exceeds the permitted use, you will need to obtain permission directly from the copyright holder. To view a copy of this license, visit <http://creativecommons.org/licenses/by/4.0/>.

This is a U.S. government work and not under copyright protection in the U.S.; foreign copyright protection may apply 2021